CORE
Metadata, citation and similar papers at core.ac.uk
Provided by Elsevier - Publisher Connector

International Journal of Heat and Mass Transfer 104 (2017) 650–657

Contents lists available at ScienceDirect

International Journal of Heat and Mass Transfer

journal homepage: www.elsevier.com/locate/ijhmt

Liquid–solid mass transfer to a rotating mesh electrode in a rotor–stator spinning disc configuration

P. Granados Mendoza [a], S.J.C. Weusten [a], M.T. de Groot [b], J.T.F. Keurentjes [a], J.C. Schouten [a], J. van der Schaaf [a,*]

[a] Eindhoven University of Technology, Eindhoven, The Netherlands
[b] Akzo Nobel Industrial Chemicals B.V., Amsterdam, The Netherlands

ARTICLE INFO

Article history:
Received 3 May 2016
Received in revised form 30 July 2016
Accepted 24 August 2016
Available online 13 September 2016

Keywords:
Rotor–stator spinning disc reactor
Rotating mesh electrode
Mass transfer coefficient
Limiting current density method

ABSTRACT

Here we present the mass transfer coefficient for liquid–solid mass transfer to a rotating mesh electrode and a smooth flat disc electrode in a rotor–stator spinning disc reactor. The mass transfer coefficients are measured with the limiting current density technique. Additionally, the torque is measured and the energy dissipation rate in the system is calculated. The volumetric mass transfer coefficient of the mesh electrode increases a factor 5 compared to that of the flat disc electrode at virtually equal energy dissipation rates. Due to the characteristics of the mesh, the mesh electrode offers 2.77 times higher electrode area than the flat disc. The mass transfer coefficients measured for the rotating mesh electrode are a factor 1.74 higher compared to the flat disc. Average Sherwood numbers are reported and a correlation is presented that predicts mass transfer rates of rotating meshes in rotor–stator spinning disc reactor configurations.

© 2016 The Authors. Published by Elsevier Ltd. This is an open access article under the CC BY license (http://creativecommons.org/licenses/by/4.0/).

1. Introduction

Electrochemical processes play an important role in the chemical industry, for instance in the production of important chemicals such as chlorine, sodium hydroxide, sodium chlorate, hydrogen, oxygen, and aluminium among others [1,2]. Due to the intrinsic characteristic of being an energy-intensive industry, there is a continuous drive for process improvement in order to increase the production rate with minimal power consumption. By increasing the current density of an electrochemical process, the rate of production proportionally increases. One of the challenges of operating at high current densities is that the rate at which reactants and/or products are transported to/from the electrode becomes the limiting step. When the limiting current density is reached, the rate of reaction can no longer be compensated with the rate of mass transport to/from the electrode and the process becomes mass transfer controlled. A further increase in the current density leads to undesired reactions at the electrodes and higher power consumption due to a steep increase in the cell potential. It is therefore desired to increase the mass transfer rate in electrochemical reactors. An option for this intensification is the use of high shear forces that promote a rapid mixing of fluids and a high surface renewal rate. A type of rotating equipment that uses these principles is the rotor–stator spinning disc reactor (RS-SDR) [3]. This reactor consists of a rotating disc in a cylindrical housing, with a typical gap distance between the rotor and the stator in the order of 1 mm. The high velocity gradient between the rotor and the stator and high shear forces cause high turbulence that intensify the gas–liquid [4–6], liquid–liquid [7] and liquid–solid [8] mass transfer, as well as heat transfer [9,10]. Moreover, due to the small reactor volume, the RS-SDR offers a fast start-up and shut down which is beneficial when intermittent production is required, e.g. at peak electricity production by wind or solar energy.

Mesh electrodes are used in industrial cells, for instance in zero gap cell configurations [11,12], where the electrode and membrane are in close contact and the mesh electrodes allow the contact with the electrolyte. Furthermore mesh electrodes offer the advantage of promoting turbulence, higher surface area and facilitating gas removal [13]. Rotating mesh electrodes have been previously studied by Sedahmed et al. [14]. These authors reported higher mass transfer coefficients for the rotating mesh than the predictions for the free disc in laminar regime. The flow pattern for the configuration used by Sedahmed et al. resembles that of a free disc, where the gap between the rotating disc and the bottom stator is very large. Alternatively, the reactor volume can be significantly reduced by using the RS-SDR configuration previously described, where the rotating disc electrode is placed at a small distance from

* Corresponding author.
E-mail address: j.vanderschaaf@tue.nl (J. van der Schaaf).

http://dx.doi.org/10.1016/j.ijheatmasstransfer.2016.08.076
0017-9310/© 2016 The Authors. Published by Elsevier Ltd.
This is an open access article under the CC BY license (http://creativecommons.org/licenses/by/4.0/).

Nomenclature

Symbols

a	fitting parameter (–)
A	area (m^2)
a_{LS}	liquid–solid interfacial area (m_i^2/m_R^3 s)
b	fitting parameter (–)
C^*	concentration of the electroactive species at the bulk (mol/m^3)
D	diffusion coefficient (m^2/s)
d_o	opening size of the mesh (mm)
d_w	wire diameter (mm)
E_{dr}	rotational energy dissipation rate (W)
F	Faraday constant (s A/mol)
i_L	limiting current density (A/m^2)
k_{LS}	liquid–solid mass transfer coefficient (m_L^3/m_i^2 s)
$k_{LS}a_{LS}$	volumetric liquid–solid mass transfer coefficient (m_L^3/m_R^3 s)
n	number of electrons transferred (–)
n_m	mesh size (mesh units/in^2)
R	radius (m)
Re	Reynolds number (Re = $\omega R^2/\nu$)
Sc	Schmidt number (Sc = ν/D)
Sh	Sherwood number, Sh = $k_{LS}R/D$

Greek letters

δ	thickness of the diffusion layer (m)
ω	rotational speed (rad/s)
ν	kinematic viscosity (m^2/s)
τ	torque (Nm)

Abbreviations

CE	counter electrode
WE	working electrode
RDE	rotating disc electrode
RS-SDR	rotor–stator spinning disc reactor

the stator which is then used as counter electrode. In practical applications the RS-SDR configuration exhibits a lower ohmic drop and therefore lower cell voltage due to the small gap distance between electrodes. This configuration resembles that of the pump cell electrolyzer that has been studied extensively by Jansson et al. for processes like metal deposition [15] and electroorganic synthesis [16]. However the use of mesh or other structured electrodes in the RS-SDR configuration has not been investigated yet.

Therefore, this paper presents liquid–solid mass transfer coefficients (k_{LS}) of a rotating mesh electrode in a RS-SDR configuration determined by measuring the limiting current density [17,18]. Furthermore, mass transfer coefficients for a flat smooth disc in the RS-SDR configuration are also reported. The values of mass transfer coefficients presented here correspond to the average values over the entire surface of the rotating mesh or rotating disc. The system investigated here corresponds to Schmidt numbers much larger than unity, for which several empirical and semi-empirical mass transfer equations have been reported. In Table 1 we present some examples of correlations reported in literature, though the list is not exhaustive. For free discs, an overview of the available equations can be found in [19].

The results obtained in this study are also reported in the form of a Sherwood correlation as a function of the Reynolds number of the type:

$$\mathrm{Sh} = a\,\mathrm{Re}^{b}\,\mathrm{Sc}^{0.33} \tag{1}$$

where Sh = $k_{LS}R/D$ is the Sherwood number, Re = $\omega R^2/\nu$ is the rotational Reynolds number and Sc = ν/D is the Schmidt number with k_{LS} being the mass transfer coefficient, R the disc radius, D the diffusion coefficient, ω the rotational speed, ν the kinematic viscosity, a and b are fitting parameters.

2. Methodology

2.1. Limiting current density method

The mass transfer coefficient was measured using the limiting current density method. When the rate of reaction is so high that the concentration at the electrode becomes zero, the limiting current density i_L is reached and the rate of reaction can be expressed by:

Table 1
Compilation of previously reported mass transfer data in the form of Sherwood correlations as functions of Reynolds and Schmidt for free discs and rotor–stator configurations and the correlations proposed in the present study.

Correlation and range of validity		Authors	Notes
Free disc in infinite liquid			
$\mathrm{Sh} = 0.62\mathrm{Re}^{0.5}\mathrm{Sc}^{0.33}$	(6)	Levich [23]	a, d
$\mathrm{Re} < 2.7 \times 10^5$			
$\mathrm{Sh} = (0.89 \times 10^5\mathrm{Re}^{-0.5} + 9.7 \times 10^{-15}\mathrm{Re}^3)\mathrm{Sc}^{0.33}$	(7)	Mohr et al. [28]	a, d
$2 \times 10^5 < \mathrm{Re} < 4 \times 10^5$			
$\mathrm{Sh} = 0.007\mathrm{Re}^{0.9}\mathrm{Sc}^{0.33}$	(8)	Daguenet [26]	b, d
$\mathrm{Re} > 2.7 \times 10^5$			
Disc in rotor–stator configuration			
$\mathrm{Sh} = 0.85\mathrm{Re}^{0.5}\mathrm{Sc}^{0.33}$	(9)	Cavalcanti et al. [27]	a, d
$87 < \mathrm{Re} < 9.7 \times 10^3, 0.1 < G < 2.26$			
$\mathrm{Sh} = 2 \times 10^{-8}\mathrm{Re}^2 + 9 \times 10^2$	(10)	Meeuwse et al. [8]	c, e
$1 \times 10^5 < \mathrm{Re} < 7 \times 10^5$			
$\mathrm{Sh} = 0.799\mathrm{Re}^{0.492}\mathrm{Sc}^{0.33}$	(11)	Present work	
$5.89 \times 10^3 < \mathrm{Re} < 2.24 \times 10^5$			
$\mathrm{Sh} = 7.27 \times 10^{-4}\mathrm{Re}^{1.055}\mathrm{Sc}^{0.33}$	(12)		
$2.24 \times 10^5 < \mathrm{Re} < 6.72 \times 10^5$			
Rotating mesh in free disc configuration			
$\mathrm{Sh} = 0.26Re^{0.5}Sc^{0.33}(R/d_w)^{0.5}$	(13)	Sedahmed et al. [14]	a, f
$5.2 \times 10^4 < Re < 3.4 \times 10^5, 35.7 < R/d_w < 92.6$			
Rotating mesh in rotor–stator configuration			
$\mathrm{Sh} = 0.892\mathrm{Re}^{0.57}\mathrm{Sc}^{0.33}$	(14)	Present work	
$5.89 \times 10^3 < \mathrm{Re} < 6.72 \times 10^5$			

Notes:
[a] Empirical correlation based on measurements of limiting current density of the reduction of ferricyanide.
[b] Empirical correlation based on measurements of limiting current density of the reduction of triiodide.
[c] Empirical correlation based on mass transfer measurements of heterogeneously catalyzed glucose oxidation.
[d] Without superposed flow.
[e] With radially inwards superposed flow.
[f] The electrode gap although not specified it was estimated to be large and therefore it was considered to be a free disc configuration with electrolyte recirculation, i.e. superposed axial flow.

$$\frac{i_L}{nF} = \frac{D}{\delta}C^* = k_{LS}C^* \tag{2}$$

where i_L is the limiting current density, n is the number of electrons transferred, F is the Faraday constant, D is the diffusion coefficient, δ

is the thickness of the diffusion layer, C^* is the concentration of the electroactive species at the bulk, and k_{LS} is the mass transfer coefficient. In a current vs potential plot, the limiting current density results in a plateau of constant current for a certain potential range. Therefore a direct measurement of the mass transfer coefficient is possible by determining the limiting current density plateau from linear sweep voltammograms and knowing the bulk concentration. Further details of this method can be found elsewhere [17,18]. In the present study the limiting current density for the reduction of hexachloroiridate (IV) [20] is investigated:

$$IrCl_6^{2-} + e^- \leftrightarrow IrCl_6^{3-} \quad (3)$$

2.2. Experimental setup

Fig. 1 shows a schematic representation of the experimental setup consisting of the rotor–stator spinning disc reactor (RS-SDR) connected to a PGSTAT30 potentiostat/galvanostat (Autolab). The RS-SDR consists of an acrylic (PMMA) housing with a disc of radius $R = 0.065$ m mounted on a rotating shaft. The rotating disc was placed at a gap distance $h = 1$ mm from the top and bottom stators forming a top and a bottom cavity. For this experimental setup the rotating disc was used as a working electrode (WE) which is the cathode in this case, and the stator as counter electrode (CE) that corresponds to the anode.

Two WE configurations were used: a smooth flat disc and a woven mesh. For the flat disc, the WE was a nickel disc (99+% purity, Salomons Metalen) of radius $R = 0.065$ m and 1 mm thickness which was casted on one side with epoxy resin to a final thickness of 3 mm. In this way only one side of the disc was electroactive. The potentiostat/galvanostat was connected to the WE via a slip ring and a Ni wire running through the hollow shaft and ending in a small Ni spring protruding 2 mm from the shaft where the rotating disc was mounted. A small incision of 2 mm was made on the centre of the disc on the epoxy side to expose the nickel metal and allow the electrical connection to the Ni spring. For the mesh WE, a circular piece of a plain weaved nickel mesh (99 +% purity, Alfa Aesar) of size $n_m = 100$, wire diameter $d_w = 0.1$ mm and opening size $d_o = 0.15$ mm was used (see Fig. 2). This mesh was mounted on a PMMA disc of $R = 0.065$ m and was secured using thin polyester thread through small holes (0.2 mm) on the disc. After securing the mesh, the small holes on the disc were closed with epoxy resin to prevent liquid penetrating through them. In the centre of the disc a small Ni insert was placed in order to allow the electrical connection between the Ni mesh and the connecting spring/wire in the same way as the disc. The disc and mesh-disc were mounted on the shaft using small insulating plastic screws. The CE consisted of a nickel disc of $R = 0.065$ m and 2 mm thickness mounted flush on the bottom stator using epoxy resin to glue both parts. A Ni rod protruding to the exterior of the PMMA bottom stator and attached to the CE served for the connection to the potentiostat/galvanostat.

The flat disc WE and CE were polished using a STRUERS grinding/polishing machine with alumina slurries down to 0.5 μm, rinsed with demineralized water and sonicated to remove alumina rests. To remove oxides H_2 gas was evolved at 10 mA/cm^2 for 15 min for both flat disc and mesh disc WE's. No further pretreatment was performed for the mesh electrode.

A peristaltic pump Masterflex-77201-60 was used to circulate the electrolyte through the reactor with flowrates up to 10 ml/s. The inlet of the liquid is from the top of the rotating cavity at the shaft as depicted in Fig. 1. The liquid then flows radially outwards through the top cavity and then radially inwards through the bottom cavity. This bottom cavity corresponds to the WE-CE gap where the electrochemical processes occur. The liquid exits the reactor through a hole in the centre of the stator. The exit line of the electrolyte serves also for connecting to a Ag/AgCl reference electrode. The electrolyte vessel allows for the recirculation of the liquid. Prior to the experiments the electrolyte was deaerated with argon flushing for 30 min. During the measurements the Ar flow was kept above the liquid level to prevent oxygen from air entering the reactor.

Electrochemical measurements were performed using the AUTOLAB software NOVA. This software was additionally used to remotely control the RS-SDR rotational speed by connecting the reactor motor to the analog voltage input/output ports of the potentiostat/galvanostat. During the experiments the rotational speed ω was varied between 0 and 132 rad/s. Records of the torque of the RS-SDR were also taken in order to estimate the energy dissipation. All experiments were performed at room temperature of 20 °C.

Electrolytes were prepared in demineralized water and 0.5 M KNO_3 (Sigma Aldrich) was used as supporting electrolyte. The concentration of the redox pair was 0.3 and 3 mM of hexachloroiridate (IV) and (III) respectively (Alfa Aesar). Electrolytes were stored in brown bottles to prevent decomposition. Electrolyte concentrations were verified by UV–Vis spectroscopy. Calibration curves and details on the UV–Vis measurements are shown in the Appendix A.

Electrolyte density and viscosity were obtained from reported literature [21]. The diffusion coefficient was obtained by measuring the limiting current density of hexachloroiridate (IV) over a small rotating disc electrode (RDE) of $R = 0.0025$ m. Details on the methodology can be found elsewhere [22]. These measure-

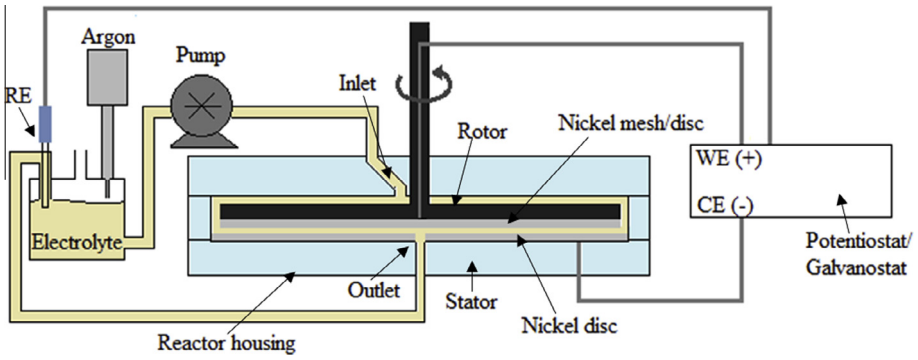

Fig. 1. Schematic representation of the experimental setup used in this study. It consists of a rotor–stator spinning disc reactor with the rotor used as working electrode and the stator used as counter electrode. The electrodes are connected to a potentiostat/galvanostat. The working and counter electrodes are discs of radius $R = 0.065$ m. The electrode gap distance $h = 1 \times 10^{-3}$ m, resulting in a gap ratio $G = h/R = 0.015$. A peristaltic pump is used to circulate the electrolyte radially inwards through the electrode gap.

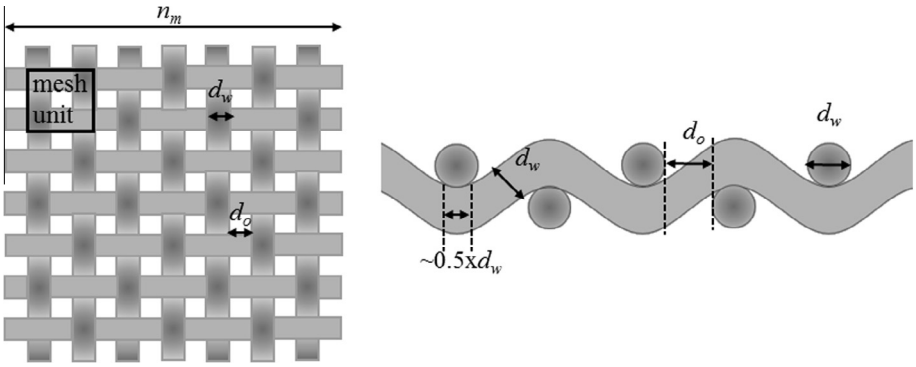

Fig. 2. Mesh characteristics and dimensions: n_m is the number of mesh units per square inch, d_w is the wire diameter and d_o is the size of the opening.

ments were carried out in a typical three-electrode cell. The WE was a nickel disc embedded in an insulating Teflon holder (Pine Instruments), the CE was a platinum wire and a Ag/AgCl electrode was used as RE. Electrode pretreatment and electrolyte concentration were the same as those described before.

3. Results and discussion

3.1. Diffusion coefficient of hexachloroiridate

According to the derivation of Levich [23] the diffusion coefficient can be experimentally obtained by determining the dependence of the limiting current density i_L on the rotational speed of a rotating disc electrode in laminar regime and free disc configuration. The Levich equation [23] is an analytical equation that describes this relationship and for a one-electron transfer reaction like the one investigated here, it can be written as:

$$\frac{i_L}{C^*} = 0.620 F \nu^{-1/6} D^{2/3} \omega^{1/2} \tag{4}$$

At the small radius of the RDE used here and for a wide range of rotational speeds (0 and 314 rad/s used in this case) the RDE is in the laminar regime where the Levich Eq. (4) is applicable [18] and the diffusion coefficient can be directly determined. Fig. 3 shows the obtained experimental results for the reduction of hexachloroiridate (IV). The experimental data was fitted to Eq. (4) and the results are in good agreement with the theoretical predictions. The resulting diffusion coefficient is $D = 8.46 \times 10^{-10}$ m^2/s. Petrovic reported a diffusion coefficient of 8.93×10^{-10} m^2/s for the reduction of hexachloroiridate (IV) in 0.1 M KNO_3. The corresponding Schmidt number is 1007, and therefore the Levich equation is applicable [19,24]. Results are in good agreement with the theoretical predictions of the Levich Eq. (4).

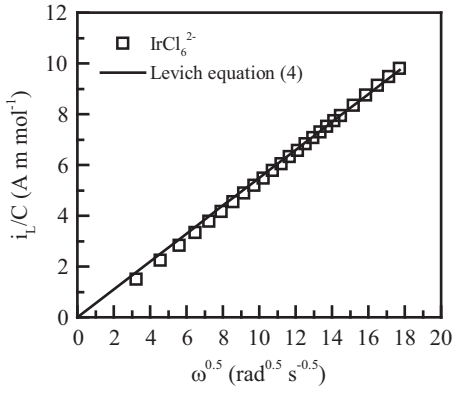

Fig. 3. Variation of the current density with $\omega^{0.5}$ for the reduction of hexachloroiridate $IrCl_6^{2-}$ on a Nickel rotating disc electrode (RDE) in a free disc configuration. Data markers □ correspond to experimental values and the solid line correspond to the results fitted to Levich Eq. (4).

3.2. Mass transfer coefficients of a flat disc and a mesh disc in RS-SDR configuration

To determine mass transfer coefficients we need to know the current density, for which we need the electroactive area. Often a distinction is made between the geometrical area of the electrode and the real surface electroactive area [25]. The latter is related to the surface roughness typically in the order of nanometers due to imperfections on the electrode surface. The real surface electroactive area is relevant for the mass transfer coefficient determination when the surface roughness is of the same order of magnitude as the diffusion layer thickness. The measurements of the mass transfer coefficient presented here, which will be discussed in the following section, indicate that the diffusion layer thickness is between 10 and 100 μm for the range of rotational speeds here investigated. Therefore the nanometer-scale surface roughness is not relevant, and for this reason the geometric area is considered for calculating the limiting current density. For the case of the flat disc, this simply corresponds to the geometrical area of the disc, i.e. $A_{disc} = 0.01327$ m^2_E. On the other hand, the area of the mesh is slightly more complicated to calculate. Considering the mesh design (i.e. a plain weaved mesh) a formula was derived to calculate the ratio of mesh surface area and the geometrical area of the disc:

$$\frac{A_{mesh}}{A_{disc}} = 0.31 \pi d_w n_m^2 \sqrt{(0.5 d_w + d_o)^2 + (2 d_w)^2} \tag{5}$$

where A is the area, d_w is the wire diameter, d_o is the opening size, n_m is the mesh size in units per square inch. Details on the derivation of Eq. (5) are shown in Appendix B. Substitution of the mesh characteristics used in this study into Eq. (5) gives a ratio of 2.77 for the area of the mesh compared to the flat geometric area, resulting in a mesh electroactive area of $A_{mesh} = 0.0367$ m^2_E.

The values of the mass transfer coefficients are obtained from the current plateaus of Linear Sweep Voltammograms as a function of the rotational speed as shown in Fig. 4. As shown in this figure, well-defined current plateaus were observed from which the limiting current can be determined. The measurements of the k_{LS} presented hereafter correspond to the average of the current measured in the range of −0.2 and −0.4 V.

The obtained k_{LS} values are shown in Fig. 5 for both flat disc and mesh electrodes as a function of the rotational speed. For both cases an increase in the k_{LS} with increasing ω is observed. An increase in the rotational speed from $\omega = 0$ to 132 rad/s results in

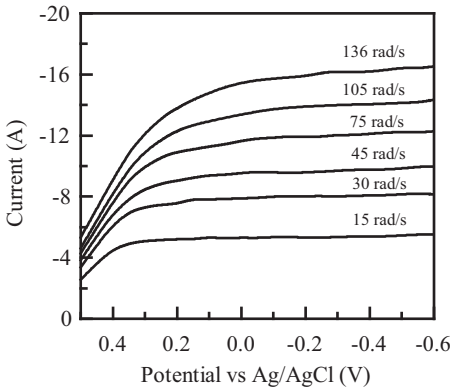

Fig. 4. Linear sweep voltammograms for the reduction of hexachloroiridate (IV) on a Ni rotating mesh electrode in RS-SDR configuration. The parameter in this figure is the rotational speed of the mesh electrode (ω in rad/s). For all rotational speeds, well-defined current plateaus are observed between −0.2 and −0.4 V vs Ag/AgCl reference electrode.

an increase of k_{LS} from 5.92×10^{-6} to 1.16×10^{-4} $m_L^3\ m_E^{-2}\ s^{-1}$ for the flat disc. For all rotational speeds, higher values of k_{LS} are obtained for the rotating mesh electrode compared to those obtained for flat disc. At the highest rotational speed measured in these experiments of ω = 132 rad/s (corresponding to a Reynolds number of $Re = 6.72 \times 10^5$) the mass transfer coefficient for the rotating mesh electrode is $k_{LS} = 2.02 \times 10^{-4}$ $m_L^3\ m_E^{-2}\ s^{-1}$ and for the rotating flat disc $k_{LS} = 1.16 \times 10^{-4}$ $m_L^3\ m_E^{-2}\ s^{-1}$. The higher k_{LS} values obtained for the rotating mesh electrode are attributed to a higher degree of turbulence and surface renewal compared to the flat disc. The mesh acts as a turbulence promoter distorting the fluid boundary layers and promoting the formation of eddies at the electrode surface.

The results obtained here can be compared to those obtained by Sedahmed et al. [14] for rotating meshes in free disc configuration. The mass transfer coefficients reported by Sedahmed et al. [14] at $Re = 3.4 \times 10^5$ range between $k_{LS,Sedahmed} = 1.3 \times 10^{-4}$ and 3.7×10^{-4} $m_L^3\ m_E^{-2}\ s^{-1}$ depending on the mesh type used. The woven meshes used by Sedahmed et al. ranged in wire diameter d_w between 0.27 to 0.71 mm in contrast to 0.1 mm used here. The size of the opening is also significantly larger for Sedahmed's work where d_o ranged between 0.59 and 1.86 mm compared to 0.15 mm used in the present work.

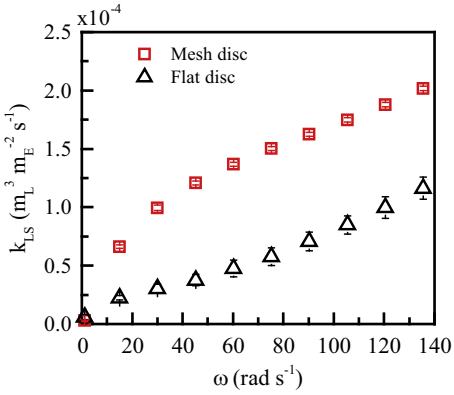

Fig. 5. Mass transfer coefficient k_{LS} as a function of the rotational speed ω based on measurements of the limiting current density according to Eq. (2) for the reduction of 0.3 mM hexachloroiridate (IV) on a Ni mesh disc (□) and a Ni flat disc (Δ) in a RS-SDR configuration. Both electrodes have radius R = 0.065 m. The electroactive area for each configuration is $A_{mesh} = 0.0367$ m_E^2 and $A_{disc} = 0.0132$ m_E^2 for the mesh and for the flat disc, respectively.

The performance of the reactor is not only given by the mass transfer coefficient k_{LS} but more importantly by the volumetric mass transfer coefficient represented by the product of the mass transfer coefficient k_{LS} and the liquid solid interfacial area per unit volume of reactor a_{LS}. The reactor volume in this case is 2.8×10^{-5} m_R^3 resulting in $a_{LS,disc} = 477$ $m_E^2\ m_R^{-3}$ and $a_{LS,mesh} = 1322$ $m_E^2\ m_R^{-3}$ for the flat disc and the mesh, respectively. The $k_{LS}a_{LS}$ values are plotted as a function of Reynolds number in Fig. 6 where it can be observed that for the highest rotational speed (ω = 132 rad/s) the volumetric mass transfer coefficient for the mesh is ~5 times higher for the mesh than for the disc. This shows evidently one of the benefits of using a rotating mesh in RS-SDR configuration for the intensification of chemical and electrochemical processes.

3.3. Mass transfer correlations

From the measured mass transfer coefficients, the corresponding Sh numbers were calculated and the data was fitted to obtain correlations as a function of the Re number. Table 1 presents a summary of the available mass transfer correlations including those proposed here.

Fig. 7a shows the results for the flat disc where two regions can be distinguished: (1) a laminar region at $Re < 2.2 \times 10^5$ and 2) a transition to turbulent region at $Re > 2.2 \times 10^5$. A power law model of the form $Sh = aRe^bSc^{0.33}$ is used to fit the experimental Sh and to obtain the mass transfer correlations for these two regions:

$$Sh = 0.799Re^{0.492}Sc^{0.33} \quad \text{for } 5.89 \times 10^3 < Re < 2.24 \times 10^5 \tag{11}$$

$$Sh = 7.27 \times 10^{-4}Re^{1.055}Sc^{0.33} \quad \text{for } 2.24 \times 10^5 < Re < 6.72 \times 10^5 \tag{12}$$

The experimental results and the fitted curves are shown in Fig. 7a. The laminar correlations of Levich [23] and the turbulent correlation of Daguenet [26] for free discs are also plotted in Fig. 7a. For $Re < 2.2 \times 10^5$ the proportionality of $Sh \propto Re^{0.492}$ is in line with the predictions for rotating discs in the laminar regime with $Sh \propto Re^{0.5}$ according to Levich [23] for free discs and Cavalcanti et al. [27] for rotor–stator configurations (Eqs. (6) and (9), respectively). The values of Sh obtained here are also close to the values predicted by the correlation of Levich (Eq. (6)). Similar dependencies have been reported for the heat transfer coefficient for the fluid-rotor heat transfer in a flow configuration similar to the one studied here [10]. The proportionality of $Sh \propto Re^{1.055}$ for $Re > 2.2 \times 10^5$ can be interpreted as a transition region. The onset of transition from

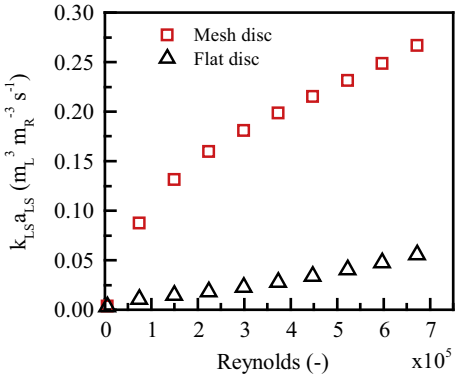

Fig. 6. Volumetric mass transfer coefficient $k_{LS}a_{LS}$ as a function of the rotational speed ω for a rotating mesh disc (□) and a rotating flat disc (Δ) in a RS-SDR configuration. The reactor volume is 2.78×10^{-5} m_R^3 and both electrodes have radius R = 0.065 m. The liquid–solid interfacial area per unit volume is $a_{LS,disc}$ = 477 $m_E^2\ m_R^{-3}$ and $a_{LS,mesh}$ = 1322 $m_E^2\ m_R^{-3}$ for the flat disc and the mesh, respectively.

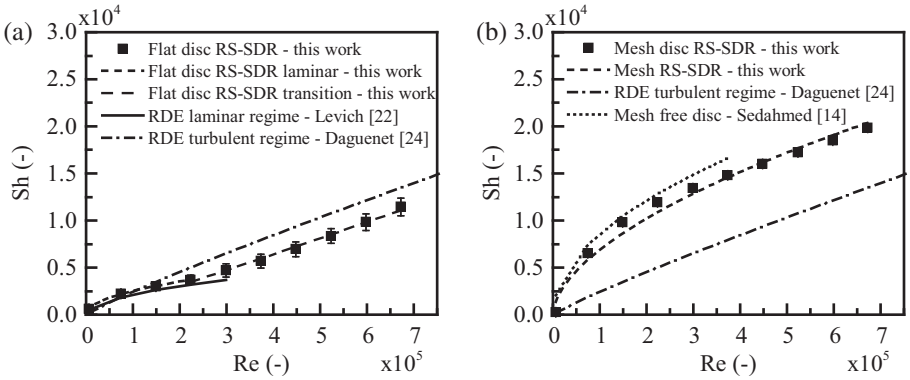

Fig. 7. Sherwood number as a function of the Reynolds number for (a) a flat disc and (b) a mesh disc, both in a RS-SDR configuration. The data markers correspond to obtained experimental data. The lines correspond to the power law fitting shown in Eqs. (11)–(14).

laminar to turbulent flow observed here is in accordance with the reported literature for rotor–stator systems where it at $Re = 2–3 \times 10^5$ [28,29]. The turbulent regime is fully developed at the rim of the disc, but at lower disc radii the regime is still in transition. This has been previously reported by Owen et al. [29] and Meeuwse et al. [8]. This explains the higher exponent of Re found here, i.e. 1.055 compared to the expected exponent 0.9 typical for rotating discs in the turbulent regime at high Sc numbers [26]. Typically in the transition region, the Sh number grows faster than in fully developed turbulent flow [19,29]. It must be noted that for lower Sc numbers, for instance for mass transfer measurements using the naphthalene sublimation technique for which the Schmidt number is in the range of 2.28–2.5, the exponent of the Re number is 0.8 [24]. Similarly for heat transfer measurements in air, with Prandtl numbers close to unity, the exponent of the Re number is 0.8 [19,29]. The correlations (6) and (7) are applicable only for the range of Re numbers indicated. At higher Re numbers it is expected that the Sh number for a flat disc will approach the predictions of Daguenet [26] for a free disc in turbulent regime.

For the case of the rotating mesh electrode a power law model is also used to obtain a mass transfer correlation. In this case, no transition between laminar and turbulent was observed as in the case of the flat disc. The obtained correlation for the mesh electrode is:

$$Sh = 0.892Re^{0.57}Sc^{0.33} \quad \text{for } 5.89 \times 10^3 < Re < 6.72 \times 10^5 \qquad (14)$$

Fig. 7b shows a comparison of the experimental results obtained with the mesh in the RS-SDR and the correlation of Daguenet [26] for free discs in the turbulent regime. It can be observed that significantly higher Sh numbers are obtained with the mesh in the RS-SDR compared to the free disc. This is the case even for low rotations, where for instance at $Re = 1.5 \times 10^5$ ($\omega = 32$ rad/s) the Sh number is increased from $Sh_{free\text{-}disc} = 0.35 \times 10^4$ for a free disc in the turbulent regime to $Sh_{mesh\text{-}RS\text{-}SDR} = 0.95 \times 10^4$ for the rotating mesh in the RS-SDR. For the case of a rotating mesh in a free disc configuration, Sedahmed et al. [14] found a proportionality of $Sh \alpha Re^{0.5}$ for Re between 5.25×10^4 and 3.40×10^5 similar to the proportionality $Sh \alpha Re^{0.57}$ found here. The proportionality of $Re^{0.5}$ found by Sedahmed and $Re^{0.57}$ found here for the rotating mesh resembles the proportionality $Re^{0.5}$ found for flat discs in laminar regime, suggesting that a similar mass transport mechanism occurs. For the case of a flat disc in laminar regime the convective flow towards the disc increases the radial outflow that increases with radius, consequently there is a convective azimuthal flow towards the disc. This flow significantly increases the mass transfer towards the disc and leads to the $Re^{0.5}$ proportionality. In the case of the rotating mesh, the open structure of increases the convective flow even more, leading to higher mass transfer and maintaining the proportionality of $Re^{0.5}$.

The correlation presented by Sedahmed et al. [14] is also a function of the ratio between the mesh radius R and the wire diameter d_w (R/d_w), as seen in equation (13). In the present study only one mesh type is used and therefore correlations as a function of the wire diameter are not attempted. The range of ratio of mesh radius and wire diameter used by Sedahmed et al. is $35.7 < R/d_w < 92.6$ whereas for the present work this results in $R/d_w = 650$ which is significantly different. Calculating using Sedahmed's correlation (Eq. (13)) for $Re = 6.72 \times 10^5$ and the mesh characteristics of this study ($R/d_w = 650$), the Sherwood number predicted is $Sh = 5.92 \times 10^4$ compared to $Sh = 1.99 \times 10^4$ obtained experimentally (Fig. 7b). Using Sedahmed's correlation for $Re = 6.72 \times 10^5$ and a maximum R/d_w ratio used by the authors ($R/d_w = 92.6$) [14], a Sherwood number of $Sh = 2.23 \times 10^4$ is obtained, which is closer to the experimental value obtained here (see Fig. 7b).

3.4. Energy dissipation

The rotational energy dissipation rate E_{dr} of the RS-SDR is calculated from the torque τ exerted on the rotor which is directly measured by the control interface of the RS-SDR and is given by:

$$E_{dr} = \omega(\tau - \tau_0) \qquad (15)$$

where τ is the torque measured while the reactor is in operation, i.e. with the electrolyte flowing through, and τ_0 is the torque of the reactor while running idle, i.e. without fluid. Results are shown in Fig. 8 where it can be observed that the energy dissipation rate for the flat disc and the mesh disc are in the same order of magnitude and practically the same for $Re < 6 \times 10^5$. At higher Reynolds numbers, E_{dr} for the mesh disc is slightly higher compared to the flat disc, being $E_{dr,mesh\text{-}disc} = 18.8$ W for the mesh disc compared to $E_{dr,flat\text{-}disc} = 16.4$ W for the flat disc at the highest Re measured ($Re = 7.8 \times 10^5$) corresponding to a rotational speed of $\omega = 157$ rad/s. These results show that the increase in energy dissipation rate by using a rotating mesh in a RS-SDR is not significant compared to the energy dissipation rate for a rotating flat disc. This means that by using a rotating mesh in a RS-SDR one can obtain significantly higher $k_{LS}a_{LS}$ (Fig. 6) than the flat disc at virtually the same energy dissipation rate (Fig. 8).

The obtained results of the energy dissipation rate are fitted to a power law model as a function of the Reynolds number and the results are given by the following equations for the mesh disc and for the flat disc respectively:

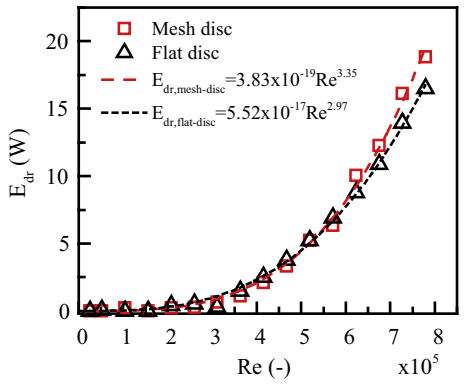

Fig. 8. Energy dissipation rate E_{dr} as a function of the Reynolds for a rotating mesh disc (□) and a rotating flat disc (Δ), both in a RS-SDR configuration. The data markers correspond to experimental data obtained by measurements of the torque τ according to Eq. (15). The lines correspond to the power law fitting shown in Eqs. (16) and (17).

$$E_{dr,mesh-disc} = 3.83 \times 10^{-19}\mathrm{Re}^{3.35} \tag{16}$$

$$E_{dr,flat-disc} = 5.52 \times 10^{-17}\mathrm{Re}^{2.97} \tag{17}$$

Similar dependence of the energy dissipation rate and the Reynolds number have been reported for rotor–stator spinning disc reactors, where De Beer et al. [9] reported a proportionality of $E_{dr}\alpha\mathrm{Re}^{2.12}$ for their measurements of single phase heat transfer in a rotor–stator spinning disc reactor.

4. Conclusions

The limiting current density for the reduction of hexachloroiridate (IV) has been used to determine liquid solid mass transfer to a rotating mesh electrode and a flat disc electrode in a rotor–stator spinning disc configurations. The k_{LS} values for both flat disc and mesh electrodes increase with increasing rotational speed. Higher k_{LS} values were obtained for the rotating mesh electrode in comparison to a flat disc, being $k_{LS} = 2.02 \times 10^{-4}\ \mathrm{m_L^3\ m_E^{-2}\ s^{-1}}$ for the mesh electrode which is a factor 1.74 higher than the flat disc at the highest rotational speed measured ($\omega = 132$ rad/s). The volumetric mass transfer coefficient $k_{LS}a_{LS}$ is found to be ~5 times higher for the mesh than for the disc. This is the result of an increase of a factor 2.77 of the mesh area compared to the disc area. For the case of the flat disc, two Sherwood correlations are presented corresponding to the laminar (Eq. (11)) and turbulent regime (Eq. (12)). The proportionalities of Sh with respect to Re agree with previously reported literature on rotating discs. For the rotating mesh electrode no transition region was perceived from the experimental measurements. Thus a single correlation is presented for the range of Re numbers investigated here (Eq. (14)) for the case of the rotating mesh. A proportionality of $\mathrm{Sh}\alpha\mathrm{Re}^{0.57}$ is found for the rotating mesh which is similar to the proportionality of $\mathrm{Re}^{0.5}$ found in flat discs in laminar regime. The increase in mass transfer for the rotating mesh can be attributed to an increase in the convective azimuthal flow towards the electrode caused by the open structure of the mesh. Measurements of the torque of the RS-SDR with the flat disc and the mesh disc showed that both configurations exhibit virtually the same energy dissipation rate. Therefore we conclude that the increase in mass transfer rates by using the rotating mesh disc in RS-SDR does not occur at the expense of an increase in the power consumption of the reactor compared to a flat disc. Moreover, for electrochemical processes the rotor stator configuration is of particular interest due to the very small interelectrode gap (in the order of 1 mm) which leads to lower ohmic drop compared to free discs where the distance between electrodes is significantly larger. These results show the potential of the RS-SDR configuration for the intensification of chemical and electrochemical processes.

Acknowledgements

This project is funded by the Action Plan Process Intensification of the Dutch Ministry of Economic Affairs (project PI-00-04). The authors acknowledge A. Colau for his assistance in the preparative experimental work. Also, the authors acknowledge M.T.M. Koper, E. Perez Gallent and I.D. Ledezma Yanez from the Leiden Institute of Chemistry, Leiden University, for their assistance with the RDE measurements.

Appendix A. Concentration determination via UV–Vis spectrophotometry

Fig. A.1 shows the UV–Vis spectrum of hexachloroiridate (III) and (IV) in the concentration range used in this study. For the redox species of interest, i.e. the hexachloroiridate (IV), peaks are observed at 415 and 486 nm. A calibration curve was made for each species from which the concentrations could be obtained.

Appendix B. Calculation of the mesh electrode area

A formula is derived to calculate the area of the mesh electrode based on its geometry and dimensions. The mesh used in this study is a plain weaved mesh as depicted in Fig. 2. We assume that the wires are cylinders of diameter d_w. The mesh design consists of woven wires that cause a curvature of the cylinders as they are woven over and under the other cylinders. This woven curvature is approximated by a triangular wave as shown in Fig. 2. To correct for the overlap between mesh wires in the junctions, $0.5 \times d_w$ is subtracted from the horizontal length $d_w + d_o$. The area of one mesh unit can then be calculated and multiplied by the number of units in the mesh n_m. The mesh area is then related to the geometrical area and this ratio becomes:

$$\frac{A_{mesh}}{A_{disc}} = 0.0031\pi d_w n_m^2 \sqrt{(0.5d_w + d_o)^2 + (2d_w)^2} \tag{18}$$

The value of n_m is also known as the mesh size and conventionally it is given by the supplier in units/in^2. The numerical factor in Eq. (18) accounts for the conversion of n_m to SI units, thus the mesh size in units/in^2 should be used directly for calculations in Eq. (18). Note

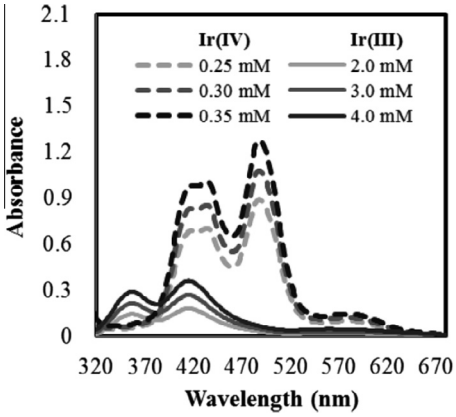

Fig. A.1. UV–Vis spectrum for aqueous solutions 0.5 M KNO_3 and hexachloroiridate (IV) (dashed lines) and hexachloroiridate (III) (solid lines) in the range of concentrations used in this study.

that d_w and d_o are given in millimeters in the above formula. For this study, the mesh type used is a woven mesh of $n_m = 100$ units/in^2 with wire diameter $d_w = 0.1$ mm and opening area $d_o = 0.1524$ mm. The resulting ratio is calculated as:

$$\frac{A_{mesh}}{A_{disc}} = 0.0031 \times \pi \times 0.1 \times 100^2 \times \sqrt{(0.5 \times 0.1 + 0.1524)^2 + (2 \times 0.1)^2} = 2.77$$

Thus, for any given geometric area, the area of the mesh electrode is 2.77 times larger.

References

[1] G.G. Botte, Electrochemical manufacturing in the chemical industry, Electrochem. Soc. Interface 49–55 (2014).

[2] C.A.C. Sequeira, D.M.F. Santos, Electrochemical routes for industrial synthesis, J. Braz. Chem. Soc. 20 (2009) 387–406, http://dx.doi.org/10.1590/S0103-50532009000300002.

[3] J. van der Schaaf, J. Schouten, High-gravity and high-shear gas–liquid contactors for the chemical process industry, Curr. Opin. Chem. Eng. 1 (2011) 84–88, http://dx.doi.org/10.1016/j.coche.2011.08.005.

[4] M. Meeuwse, J. van der Schaaf, B.F.M. Kuster, J.C. Schouten, Gas–liquid mass transfer in a rotor–stator spinning disc reactor, Chem. Eng. Sci. 65 (2010) 466–471, http://dx.doi.org/10.1016/j.ces.2009.06.006.

[5] M. Meeuwse, J. van der Schaaf, J.C. Schouten, Mass transfer in a rotor−stator spinning disk reactor with cofeeding of gas and liquid, Ind. Eng. Chem. Res. 49 (2010) 1605–1610, http://dx.doi.org/10.1021/ie901301m.

[6] M. Meeuwse, E. Hamming, J. van der Schaaf, J.C. Schouten, Effect of rotor–stator distance and rotor radius on the rate of gas–liquid mass transfer in a rotor–stator spinning disc reactor, Chem. Eng. Process. Process Intensif. 50 (2011) 1095–1107, http://dx.doi.org/10.1016/j.cep.2011.05.022.

[7] F. Visscher, J. van der Schaaf, M.H.J.M. de Croon, J.C. Schouten, Liquid–liquid mass transfer in a rotor–stator spinning disc reactor, Chem. Eng. J. 185–186 (2012) 267–273, http://dx.doi.org/10.1016/j.cej.2012.01.002.

[8] M. Meeuwse, S. Lempers, J. van der Schaaf, J.C. Schouten, Liquid−solid mass transfer and reaction in a rotor−stator spinning disc reactor, Ind. Eng. Chem. Res. 49 (2010) 10751–10757, http://dx.doi.org/10.1021/ie1003366.

[9] M.M. de Beer, L. Pezzi Martins Loane, J.T.F. Keurentjes, J.C. Schouten, J. van der Schaaf, Single phase fluid-stator heat transfer in a rotor–stator spinning disc reactor, Chem. Eng. Sci. 119 (2014) 88–98, http://dx.doi.org/10.1016/j.ces.2014.08.008.

[10] M.M. de Beer, J.T.F. Keurentjes, J.C. Schouten, J. van der Schaaf, Intensification of convective heat transfer in a stator–rotor–stator spinning disc reactor, AIChE J. 61 (2015) 2307–2318, http://dx.doi.org/10.1002/aic.14788.

[11] T.F. O'Brien, T.V. Bommaraju, F. Hine, Handbook of Chlor-Alkali Technology, Springer US, Boston, MA, 2005, http://dx.doi.org/10.1007/b113786.

[12] D. Pletcher, X. Li, Prospects for alkaline zero gap water electrolysers for hydrogen production, Int. J. Hydrogen Energy 36 (2011) 15089–15104, http://dx.doi.org/10.1016/j.ijhydene.2011.08.080.

[13] D. Pletcher, F.C. Walsh, Industrial Electrochemistry, Springer Netherlands, Dordrecht, 1993, http://dx.doi.org/10.1007/978-94-011-2154-5.

[14] G.H. Sedahmed, M.Z. Al-Abd, Y.A. El-Taweel, M.A. Darwish, Liquid–solid mass transfer behaviour of rotating screen discs, Chem. Eng. J. 76 (2000) 247–252, http://dx.doi.org/10.1016/S1385-8947(99)00172-2.

[15] G.A. Ashworth, P.J. Ayre, R.E.W. Jansson, Production of metal powders in a pump cell, Chem. Ind. (1975) 382–383.

[16] F.B. Thomas, P.A. Ramachandran, M.P. Dudukovic, R.E.W. Jansson, Laminar radial flow electrochemical reactors. III. Electroorganic synthesis, J. Appl. Electrochem. 19 (1989) 856–867, http://dx.doi.org/10.1007/BF01007933.

[17] J.R. Selman, C.W. Tobias, Mass-transfer measurements by the limiting-current technique, in: Adv. Chem. Eng, Elsevier, 1978, pp. 211–318, http://dx.doi.org/10.1016/S0065-2377(08)60134-9.

[18] A.J. Bard, L.R. Faulkner, Electrochemical Methods, second ed., John Wiley & Sons, New York, NY, 2000.

[19] I.V. Shevchuk, Convective Heat and Mass Transfer in Rotating Disk Systems, Springer, Berlin Heidelberg, Berlin, Heidelberg (2009), http://dx.doi.org/10.1007/978-3-642-00718-7.

[20] S. Petrovic, Cyclic voltammetry of hexachloroiridate (IV): An alternative to the electrochemical study of the ferricyanide ion, Chem. Educ. 5 (2000) 231–235, http://dx.doi.org/10.1007/s00897000416a.

[21] T. Isono, Density, viscosity, and electrolytic conductivity of concentrated aqueous electrolyte solutions at several temperatures. Alkaline-earth chlorides, lanthanum chloride, sodium chloride, sodium nitrate, sodium bromide, potassium nitrate, potassium bromide, a, J. Chem. Eng. Data 29 (1984) 45–52, http://dx.doi.org/10.1021/je00035a016.

[22] J.C. Bazán, A.J. Arvia, The diffusion of ferro- and ferricyanide ions in aqueous solutions of sodium hydroxide, Electrochim. Acta 10 (1965) 1025–1032, http://dx.doi.org/10.1016/0013-4686(65)80014-7.

[23] V. Levich, Physicochemical Hydrodynamics, Prentice-Hall, Englewood Cliffs N. J, 1962.

[24] I.V. Shevchuk, Turbulent heat and mass transfer over a rotating disk for the Prandtl or Schmidt numbers much larger than unity: an integral method, Heat Mass Transfer 45 (2009) 1313–1321, http://dx.doi.org/10.1007/s00231-009-0505-x.

[25] J.M. Doña Rodríguez, J.A. Herrera Melián, J. Pérez Peña, Determination of the real surface area of Pt electrodes by hydrogen adsorption using cyclic voltammetry, J. Chem. Educ. 77 (2000) 1195, http://dx.doi.org/10.1021/ed077p1195.

[26] M. Daguenet, Etude du transport de matiere en solution, a l'aide des electrodes a disque et a anneau tournants, Int. J. Heat Mass Transfer 11 (1968) 1581–1596, http://dx.doi.org/10.1016/0017-9310(68)90040-9.

[27] E.B. Cavalcanti, F. Coeuret, Mass transfer between a liquid and a binary rotating/fixed disc system in a closed cylinder, J. Appl. Electrochem. 26 (1996) 655–663, http://dx.doi.org/10.1007/BF00253465.

[28] C.M. Mohr, Mass transfer to a rotating disk in transition flow, J. Electrochem. Soc. 123 (1976) 1687, http://dx.doi.org/10.1149/1.2132668.

[29] J.M. Owen, R.H. Roger, Flow and heat transfer in rotating-disc systems. Volume I – Rotor–stator systems, Res. Support. Roll. Royce (1989), accessed October 28, 2015, http://adsabs.harvard.edu/abs/1989STIA...90457590.